Hybrid Graphical Filter Design for Reflected Wave Phenomenon in Long-Cable-Fed Motor Drives

Masayuki Hijikata, Kushan Choksi, Yuxuan Wu, Deepi Singh and Fang Luo

Department of Electrical and Computer Engineering

Stony Brook University

Stony Brook, USA

masayuki.hijikata@stonybrook.edu

Abstract—A hybrid Smith chart-based dV/dt filter design method is presented to mitigate voltage reflections in long-cable-fed motor drives. This method overcomes the challenge of applying PWM signals (or non-singular frequency signals) onto a Smith chart and enables its impedance-matching philosophy without involving complex transfer functions. The approach starts with 1st-order damping filters to ensure the accuracy of the proposed method compared to the conventional transfer function approach. It then extends to the widely adopted 2nd-order RLC dV/dt filter topology to derive the optimum filter coefficient values. Additionally, the reconfiguration circuit technique is presented to perform filter and load parasitic analyses, providing new insights into filter topologies.

Index Terms—RWP, reflected wave, voltage overshoot, overvoltages, PWM signals, Smith chart, motor drive, damping filter, dV/dt filter

I. Introduction

Overvoltages in motor drives due to impedance mismatching are known as the Reflected Wave Phenomenon (RWP) [1]. Besides reactors and sine-wave filters [2], the literature uses passive and active dV/dt filters to mitigate overvoltages [3]–[5]. In addition to the commonly adopted 2nd-order dV/dt filter for motor drives (Fig. 1c), passive 1st-order damping filters (Figs. 1a and 1b) can also be effective in long-cable-fed systems [3], [6].

Since the emergence of Wide-Band-Gap (WBG) devices, high-speed motor drive applications, and low-inductance motor applications have been explored to take advantage of these new technologies [7]. Despite their advantages of reducing switching losses and increasing power density, RWP in power cables, on the other hand, has increased profoundly [8]. This is due to the fact that these WBG devices have much higher dV/dt and operate at a much higher switching frequency; higher voltage overshoots are pronounced in the system [1].

The state-of-the-art filter designs should be able to ensure over-voltage damping without sacrificing the advantages of WBG technology. However, conventional transfer function-based filter designs will be further complicated if different loads and parasitics are involved in addition to their cable models [9].

Therefore, the investigation of different filter topologies was conducted using a hybrid graphical approach such as a Smith chart [10]. This is because a Smith chart itself is the graphical representation of transmission line equations, manipulating

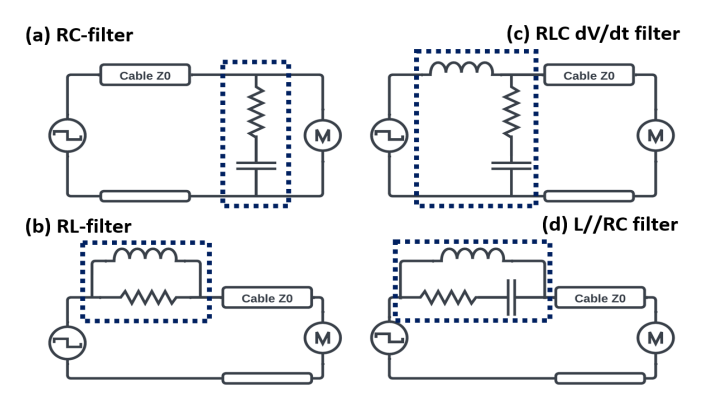


Fig. 1. Filter topologies in single-phase equivalent

graphical paths is equivalent to calculating complex mathematical equations. Although there are several challenges that need to be considered when using a Smith chart for motor drives, it has well-known properties to design impedance-matching networks used in RF engineering [11].

This paper provides a link between the transfer function and the RF impedance matching approach, which makes filter design easily extensible. In Section III, a hybrid approach to design filters using a Smith chart is described. Based on the Smith-chart results, a brief summary of effective coefficient computations for each filter is given. This will develop a methodology that can be universally applied to different filter topologies and locations, as well as cable lengths, without requiring major mathematical modifications.

II. THEORETICAL BACKGROUND

A. RWP Frequency and DM Surge Impedance

In order to highlight the advantage of using a graphical approach, this section explains several key equations used in this paper. It will be necessary to extract the characteristic impedance Z_0 and the propagation delay t_d of the cable using an impedance analyzer. The characteristic impedance of the cable is defined in the transmission line theory [11], which consists of a cascaded LC circuit with small parasitic resistance and conductance as follows:

$$Z_0 = \sqrt{\frac{R_0 + j\omega L_0}{G_0 + j\omega C_0}} \quad \approx \sqrt{\frac{L_0}{C_0}} \quad \text{(Lossless)}$$
 (1)

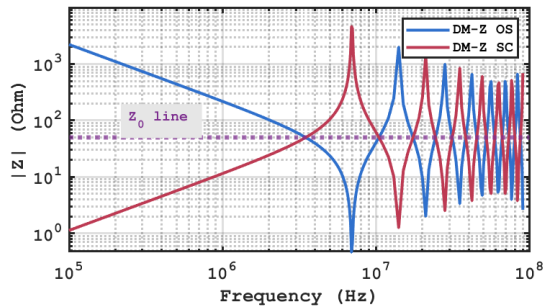


Fig. 2. Impedance of cascaded LC circuits

An open (OC) and a short (SC) circuit of Differential-Mode impedance (DM-Z) graph can be simulated using the recurrent relation of the lossless cascaded cable model as:

$$Z(n) = j\omega L_0 + \left(\frac{1}{j\omega C_0} + \frac{1}{Z(n-1)}\right)^{-1}$$
 (2)

where n is the number of cascaded elements. The initial condition for DM-Z OC is $Z(1)=sL_0+sC_0$, and DM-Z SC is $Z(1)=sL_0$. By taking the limit of Eq. (2), the constant Z_0 points can be seen at the intersection points of OC and SC lines in Fig. 2 [12]–[14]. The lower frequency parts of DM-Z OC dominate the accumulated capacitance of the cable C_c , whereas the lower frequency parts of DM-Z SC dominate the accumulated inductance of the cable L_c .

The RWP frequency of the cable in the length of l_c is associated with the propagation delay t_d of the cable as [15]:

$$t_d = l_c \sqrt{L_0 C_0} = \sqrt{L_c C_c} \tag{3}$$

$$f_{RWP} = \frac{1}{4t_d} \tag{4}$$

The 1st peak overvoltage level at the load-side, denoted as $V_L(2t_d)$ during the period $t_d \sim 3t_d$ (after two propagation delays), is described using the load and source reflection coefficients (Γ_L and Γ_S , respectively) of the system [16].

$$V_L(2t_d) = (1 + \Gamma_L)V^+ = (1 + \Gamma_L)\frac{(1 - \Gamma_S)}{2}V_{DC}$$
 (5)

$$\Gamma_L = \frac{Z_L - Z_0}{Z_L + Z_0}, \quad \Gamma_S = \frac{Z_S - Z_0}{Z_S + Z_0}$$
(6)

As the incident voltage V^+ reflects back to the source side and rebounds four times, forming a single frequency period [15], the lowest resonant frequency of the DM-Z graph in Fig. 2 indicates the RWP frequency point of Eq. (4). Here, Z_L and Z_S represent the load and source impedance of the system, respectively. In the RWP filter design, either Z_L or Z_S will be replaced by the impedance of the filter, depending on its location.

Determining accurate reflection coefficients is one of the key components for predicting voltage overshoot at the load side in Eq. (5). This is not a problem when the input voltage has a singular frequency. However, in the case of motor drive systems, the input voltages are Pulse Width Modulation (PWM) signals (or trapezoidal signals). Therefore, the traditional transfer function approach is preferable for conventional passive RWP filter designs.

B. Conventional Filter Design Approach

a) RC and RL Filters: The effective RC damping filter at the motor terminal was derived in [3]. The expected overshoot with an RC filter is expressed by Eq. (5) as follows:

$$V_L(2t_d) = (1 + \Gamma_L)V^+ = \left(2 - \frac{2Z_0}{R + Z_0} \exp^{-\frac{t}{C(R + Z_0)}}\right)V^+$$
(7)

The idea is to reduce the reflected voltage by increasing the critical rising time with the filter capacitor.

$$t_{cr} = 3t_d \frac{\Gamma_L}{\Gamma_{target}} \tag{8}$$

By assigning the critical time of the target over-voltage level, the RC coefficient formula can be derived as:

$$C_f = -\frac{3t_d}{2Z_0 \ln(1 - \Gamma_{target})} \quad , R_f = Z_0$$
 (9)

There are a few variations of this capacitor formula [16], [17], but the principle equations remain the same as Eq. (5).

Similarly, the expression for an RL filter at the source side is as follows:

$$V_L(2t_d) = (1 + \Gamma_L)[2 - (\frac{2R}{R + Z_0}) \exp^{-t\frac{Z_0 R}{L(Z_0 + R)}}]V_{DC}$$
 (10)

Thus, the desired filter coefficients can be derived by assigning the target over-voltage as [18], [19]:

$$L_f = -\frac{t_d Z_0}{\ln[2(1 - \frac{1 + \Gamma_{target}}{1 + \Gamma_L})]} , R_f = Z_0$$
 (11)

Despite the fact that the RC filter can achieve the most effective over-voltage damping at the load side, the high dissipation of heat in damping resistors is a concern [1]. On the other hand, the alternative RL filter can achieve much higher filter efficiency while compromising the over-voltage mitigation limited by the amount of inductor that can be placed in front of the cable [6].

b) RLC dV/dt Filter: By far the most commonly adopted dV/dt filter in motor drives is the series RC-type RLC filter (Fig. 1c). The advantage of this type of filter is to provide the lowering effect of dV/dt at the motor side while maintaining the minimum effect at the inverter side. The transfer function of the RLC filter is derived as follows:

$$H(s) = \frac{1 + sR_fC_f}{1 + sR_fC_f + s^2L_fC_f}$$
 (12)

Although the filter itself has the exact time-domain function [20], obtaining the time-domain function, including Eq. (5), is challenging. Multiple interpretations of this filter have been explored to determine the cutoff frequency point with the given cable parameters [3], [16], [21], [22]. Beyond these considerations, different load parasitic components make the computation of filter coefficients even more complex.

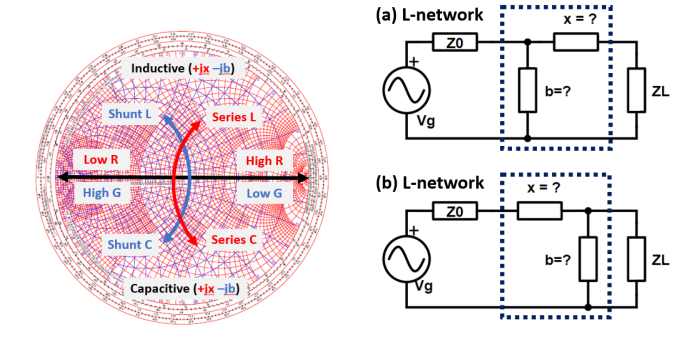


Fig. 3. A Smith chart (left) and L-network Circuits (right)

III. PROPOSED FILTER DESIGN METHODOLOGY

A. Overview

The proposed graphical filter design derives the boundary condition of each filter, so that the condition aims to achieve the following objectives:

- Find the minimum required filter coefficients for RC, RL, and RLC filters based on the given Z_0 and t_d , using the proposed equivalent ω_{eq} methods (Eq. 17 and 19).
- Find the impact of filter coefficient values with a given inductance, as well as the acceptable parasitic component values, using the proposed circuit reconfiguration-based L-network matching approach (Hybrid L-matching).

B. Smith Chart and its Properties

A Smith chart is a graphical representation of reflection coefficients in a complex gamma plane, used to solve transmission line and impedance-matching problems, mainly in RF engineering [10], [11]. In Fig. 3-left, the unit gamma circle represents impedance and admittance graphs. The impedance graph (red circles) and the admittance graph (blue circles) are inversely proportional to each other. Series reactance elements x are on the impedance graph, and shunt susceptance elements y are on the admittance graph. Moving upward on the circles indicates the value becomes more inductive, while moving downward indicates the value becomes more capacitive.

The graph's midpoint corresponds to the normalized characteristic impedance $Z_{0N}=1$ (or the impedance of interest to be matched). Points along the leftward direction of the black line indicate resistance values approaching a short circuit, while those moving in the rightward direction indicate values approaching an open circuit. The magnitude of the reflection coefficient $|\Gamma|$ is represented by the radius of the unit circle (also refer to Fig. 4-left).

Another graphical property of a Smith chart is its ability to graph the Q-factor of L-network circuits (Fig. 3-right), which is used for impedance matching between the cable and the load. Reactive components create peak resonance, and the nodal and loaded Q factors are often used to estimate the maximum signal quality within the target bandwidth.

$$Q_{loaded} = \frac{f_0}{BW} \tag{13}$$

where BW is the bandwidth of resonance frequency f_0 . The constant nodal Q-factor lines are used to estimate the loaded Q-factor by taking the ratio of reactance over resistance (x/r) or susceptance over conductance (b/g) as shown in Fig. 4-right.

Designing RWP filters using a Smith chart faces several challenges. One such challenge is its reliance on a singular frequency, limiting its applicability to narrow frequency bands for impedance matching, while the PWM voltage generated by inverters contains multiple resonant frequencies. Furthermore, deriving filter coefficients for complex filter topologies poses another challenge. Well-defined L-network matching involves a single component configured either in series or shunt at any given time. For instance, the RC filter consists of a resistor and a capacitor in series placed in parallel with the load. Given these challenges, new approaches are necessary.

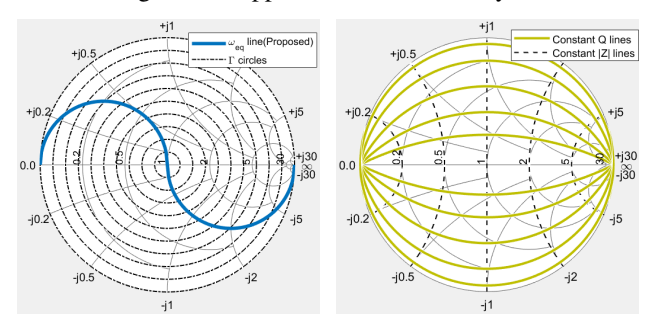


Fig. 4. ω_{eq} line with Γ circles (left) and Constant Q-factor and Z lines(right)

C. Minimum Required Coefficients for RC and RL Filters

For impedance-matching purposes, $R=Z_0$ is frequently chosen for RC and RL filters, whose impedances can be plotted on the blue line in Fig. 4-left. In the transfer function approach, the time domain functions of each reflection coefficient can be simplified in the normalized Γ_N form:

$$\Gamma_{RC} = \left(1 - e^{-\frac{t}{2Z_0C}}\right)$$
 RC filter (14a)

$$\Gamma_{RL} = \left(e^{-\frac{Z_0}{2L}t} - 1\right) \qquad \text{RL filter} \tag{14b}$$

$$\Gamma_N = \pm (1 - e^{-\frac{t}{2\tau}}) \tag{14c}$$

where 2τ is the time constant of the normalized reactive component $(2C_N \text{ or } 2L_N)$. The challenge with a Smith chart is determining which frequency to use for calculating the reflection coefficient. In this particular case, this study has identified a close approximation of Eq. (14c) on a Smith chart by using the equivalent angular frequency of:

$$\omega_{eq} = \frac{4}{\pi T}$$
 (For RC and RL filters) (15)

This approximation approach ensures the accuracy of the calculations for $(1 + \Gamma_L)$ and $(1 - \Gamma_S)$ in Eq. (5), with a mean absolute %error of less than 2% (also see Appendix A).

When considering Γ at $T=2t_d$ point, the corresponding ω_{eq} value becomes $2/\pi t_d$, and the normalized filter values can be expressed as:

$$Z_{filter} = 1 - j/\omega_{eq}C_N = 1 - j\pi t_d/2C_N$$
 RC filter (16a)

$$Y_{filter} = 1 - i/\omega_{eq}L_N = 1 - i\pi t_d/2L_N$$
 RL filter (16b)

By specifying the magnitude of reflection coefficient on Γ circles, then reading the value of intersecting X and B, the necessary coefficient of each filter will be determined as:

$$C_{filter} = \frac{-\pi t_d}{2XZ_0} = \frac{-\pi}{2X} \cdot C_{cable}$$
 RC filter (17a)

$$L_{filter} = \frac{-\pi t_d Z_0}{2B} = \frac{-\pi}{2B} \cdot L_{cable} \qquad \text{RL filter} \qquad (17b)$$

Each filter coefficient value in Eq. (17) is expressed as a multiplication of the cable's capacitance or inductance times a specific factor. For example, according to the results in Table I, achieving a 20 percent voltage overshoot at the load side would require the filter reactive value at least 3.85 times higher than the corresponding cable reactance. Using the transfer function approach, the required value would be 4.48 times, and the difference between the two approaches for overvoltage would result in MAPE of less than 2%.

TABLE I MINIMUM REQUIRED COEFFICIENT TABLE FOR RC AND RL FILTERS

$ \Gamma $ on Smith chart	0.01	0.05	0.1	0.2
X with ω_{eq} [Ω]	-0.02	-0.1001	-0.201	-0.4082
C_{filter} [times]	x78.54	x15.7	x7.82	x3.85
B with ω_{eq} [S]	-0.02	-0.1001	-0.201	-0.4082
L_{filter} [times]	x78.54	x15.7	x7.82	x3.85

D. RLC dV/dt Filter Coefficient

One challenge in computing RLC filter coefficients is determining the proper cutoff frequency point based on the cable. Especially, the topology results in the incident voltage and reflected voltage facing different impedances. If $R=Z_0$ is chosen, this study has identified a method to determine the longest propagation delay of the cable (cable length) for a given set of RLC filter coefficients on the Smith chart.

The example Smith chart plots of a critically damped RLC filter are presented in Fig. 5. The green dots on both Zin and Zout graphs indicate the filter impedance at $\omega_c = 2\pi f_c$, which is the cutoff frequency. The black dots on both graphs indicate the impedance with the same filter coefficients at the longest possible cable propagation delay before it starts to peak on the load side, calculated using the equivalent angular frequency:

$$\omega_{eq} = \frac{1}{\pi t_d}$$
 (For RLC filter) (18)

In the Zin graph (Fig. 5-left), the filter cutoff frequency point (green dot) aligns with the $Q_n = \sqrt{2}$ line (yellow line) intersecting the $R=Z_0$ circle (pink circle), while the propagation delay point (black dot) lies on the $Q_n = 1$ line. Conversely, in the Zout graph (Fig. 5, right), the filter cutoff frequency corresponds to the $Q_n = \sqrt{0.5}$ line (yellow line), and the propagation delay (black dot) is again positioned on the $Q_n = 1$ line.

Reversing graphical paths to meet the above conditions with minimal capacitance yields the RLC filter coefficient formula to achieve $Q_n \approx 1$ on both graphs. An alternative capacitor formula ($Q_n \approx 0.9$) was also given but it will break the symmetric relationship than the $Q_n \approx 1$ formula.

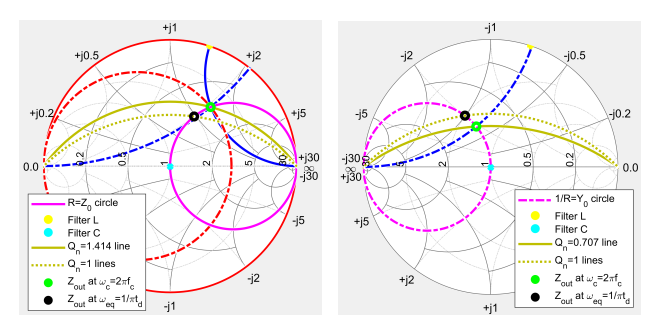


Fig. 5. Zin plot (left) and Zout plot (right) of a RLC filter

$$\begin{split} L_{filter} &= \frac{Imag(0+j1)Z_0}{\omega_{eq}} = \pi t_d Z_0 = \pi L_{cable} \\ C_{filter}^{Qn\approx 1} &= \frac{-1}{Imag(1-j0.0125)} \frac{1}{\omega_{eq} Z_0} = \frac{80\pi t_d}{Z_0} = 80\pi C_{cable} \end{split}$$

$$C_{filter}^{Qn\approx 1} = \frac{-1}{Imag(1-j0.0125)} \frac{1}{\omega_{eq} Z_0} = \frac{80\pi t_d}{Z_0} = 80\pi C_{cable}$$
 (19b)

$$C_{filter}^{Qn\approx 0.9} = \frac{-1}{Imag(1-j0.125)} \frac{1}{\omega_{eq} Z_0} = \frac{8\pi t_d}{Z_0} = 8\pi C_{cable} \tag{19c}$$

The filter capacitor formula is still subject to debate, as both the transfer function and Smith chart analysis indicate that this topology requires a higher capacitance to achieve no overvoltage $(Q_n = 1 \text{ on both graphs, also see Appendix B}).$

E. Ordinary L-matching and Hybrid L-matching

The L-network matching is one of the impedance matching methods that use one series and one parallel reactive component (an inductor or a capacitor) in an L-shape configuration to match the impedance between the source and load.

Fig. 3-right shows the two typical L-network circuits, and Fig. 6-left shows an example L-matching process graphically. The mathematical equivalent of the L-matching process is:

$$z_{LN} = (r - jx)/z_0$$
 Step (1)

$$z_1 = z_{LN} + jX_{Lnet} = 1 + jx_1$$
 Step (2)

$$y_2 = \frac{1}{z_1} + jB_{Lnet} = 1$$
 Step (3 & 4)

When an inductive load is added to the cable, the matching network is usually considered between the cable Z_0 and the inductive load Z_L . In this case, the ordinary L-network method does not seem to be applicable to the RC damping filter in Fig. 3-right (a). However, if this circuit is reconfigured with the reactive load as a part of susceptance L-matching component B_{Lnet} , and the damping resistor of the RC filter is set as a resistive load Z_L , then this circuit can be seen as an L-network circuit. In this view, the problem of finding the matching coefficients become "What RC coefficient gives the reactive load value" as shown in Fig. 6-right. The mathematical equivalent of the Hybrid L-matching process will be:

$$y_{LN} = z_0/(z_0 \pm jX_{load})$$
 Step (1 & 2) (20a)

$$z_{filter} = \frac{1}{y_{LN}} = R_{filter} \mp j X_{filter}$$
 Step (3 & 4) (20b)

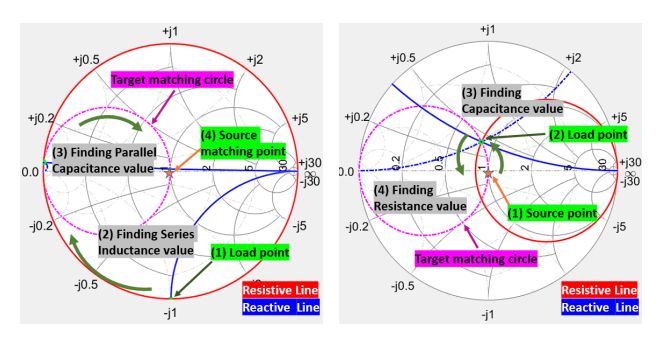


Fig. 6. Ordinary L-matching (left) and Hybrid L-matching (right)

In this way, the Zin looking into the load will be matched with Z_0 (or the target impedance) at the given frequency.

F. Parasitic Analysis with Hybrid L-matching

The impact of load inductance and its parasitic analysis can be observed using the Hybrid L-matching approach. The previously explored ω_{eq} method can be used for the target frequency, but for methodological demonstration purposes, here the omega term is defined as $\omega=2\pi f_{RWP}$. The nodal Q factor can be used to check for wide bandwidth coverage of the extracted coefficients. For instance, consider a scenario where a 130uH low-inductive load is added to a 50-ohm cable with an RC filter. After using the hybrid L-matching method, the new RC filter coefficients with the load inductance are presented in Table II. By comparing the new coefficient values with the minimum required coefficients from Table I, it can be determined whether the impact of the load is significant.

	L_{load} 130uH						
RWP Freq [MHz]	0.1 0.2 0.5 1 2 10						
Filter R [Ohm]	36.37	45.72	49.26	49.8	49.95	50	
Filter C [nF]	71.5	56.9	52.8	52.2	52.1	52	
Q_n	0.61	0.31	0.12	0.06	0.03	0.01	

As the target RWP frequency increases, the values of the matching filter capacitor approach $C_{filter} \approx L_{load}/Z_0^2$ (similar to the concept of the 'Constant Resistance Network' [25]), and with the matching condition, the inverter output will perceive the load as purely resistive. The graphical image of inductive load values affecting the RC filter coefficient values is shown in Fig. 7.

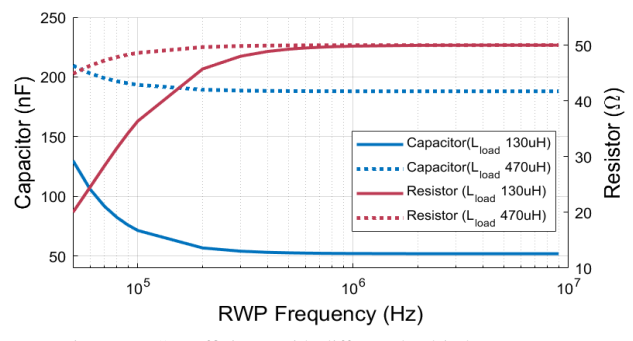


Fig. 7. RC coefficients with different load inductances

a) Effect of load EPC: In many practical situations, motors contain crucial parasitic elements such as Equivalent Parallel Capacitance (EPC), which impact cable impedance and the behavior of RWP [23], [24]. Including this parameter in the RC coefficient calculation reveals the threshold for the second resonance point. After incorporating the EPC value into the hybrid L-matching calculation, it becomes evident that if the cable possesses a specific resonance RWP frequency (or propagation delay), the system will perceive the load as capacitive (Table III). Consequently, an additional resonance peak associated with the load's EPC arises. While this effect can be offset by reducing the filter R according to the matching coefficient, the effectiveness of the RC filter may be compromised due to the matching coefficient's requirement of an inductive component. This method can also be used for parasitics of the filter resistor and inductor on the inverter side, which also impact RWP [19], [26], [27].

 $\begin{tabular}{ll} TABLE~III\\ An example of Load~EPC~Influence \end{tabular}$

	L_{load} 470uH with EPC 0.4nF							
RWP Freq [MHz]	0.1	0.1 0.2 0.3 0.4 0.5 0.6						
Filter R [Ohm]	48.8	49.82	49.98	50	49.96	49.89		
Filter C [nF]	208	268	566	-	-	-		
Filter L [uH]	-	-	-	0.15	0.46	0.62		

b) RL filter and L//RC filter: The hybrid L-matching approach can serve not only to analyze these parasitics but also to mitigate the sharp peak generated by the RL filter. By incorporating the suggested capacitive value in series with the damping resistor (Table IV), the L//RC filter topology can be realized (Fig. 1d). This topology can be beneficial in scenarios where a limited amount of filter inductance is preferred due to the inductive voltage drop across the load.

TABLE IV
AN EXAMPLE OF L//RC FILTER COEFFICIENT EXTRACTIONS

	L_{filter} value with respect to L_{cable}					
Filter L [times]	x1	x2	x5	x10	x20	x50
Filter L [uH]	2.84	5.68	14.2	28.4	56.8	142
Filter R [Ohm]	35.58	45.4	49.2	49.8	49.98	49.99
Filter C [nF]	1.6	2.5	5.8	11.4	22.7	56.8
Q_n	0.6	0.32	0.13	0.06	0.03	0.01

IV. FILTER DESIGN SIMULATION

To validate the filter design methods discussed in the previous section, a simulation-based validation was conducted. In the SPICE simulation, a 600V-10A half-bridge double pulse test with a 200kHz switching frequency was performed on the SiC evaluation board (KIT8020CRD8FF1217P-1). The simulated setup included a 50-ohm, 20ns propagation-delay cable along with a 370uH inductive load. The simulation results for various filter topologies are presented in Table V, and the corresponding waveform results are shown in Figs. 8 and 9. All filters used the damping resistor value of 50 ohms.

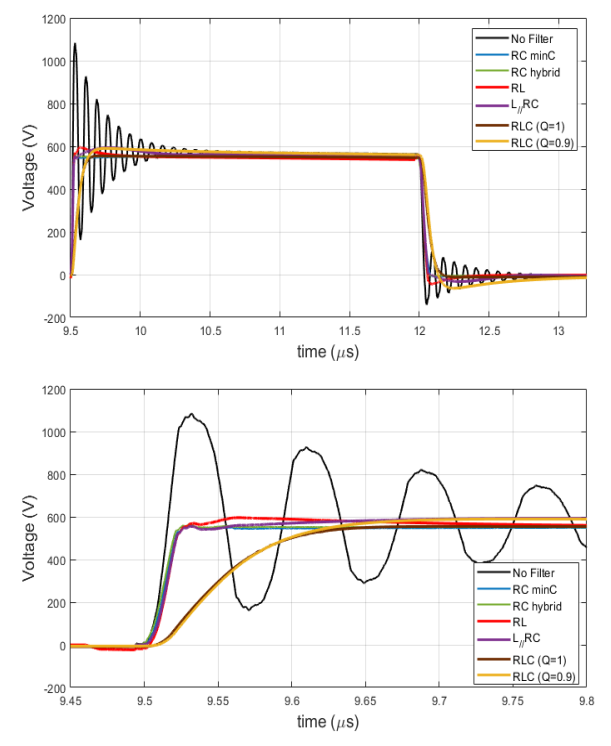


Fig. 8. Voltage at load far-view (top) and close-view (bottom)

For the RC filters, two different filter coefficients were extracted using two methods (RC minC and RC hybrid). The first method utilized the minimum filter capacitance of 30nF to achieve $\Gamma=0.01$ (a 1% voltage peak). The second method employed a filter capacitance of $148\mathrm{nF}$, obtained from the hybrid L-matching method with the 370uH load inductance. Both RC filters reduced Eon switching loss, whereas Eoff switching loss varied due to the current increase within the same switching frequency. This indicates that the hybrid L-matching results in the inverter output perceiving the load as a resistive load.

For the RL filter and the L//RC filter, the same 7.8uH filter inductor value was chosen based on the minimum filter inductance to achieve $\Gamma=0.1$ (a 10% voltage peak). The filter capacitance value of 3nF for the L//RC filter was extracted using the hybrid matching method with the same filter inductance value. Both filters achieved high filter efficiency with the targeted damping results, while L//RC reduced the peak by nearly half.

Lastly, two RLC filters with different capacitance values were simulated. The first RLC filter used the proposed method to achieve the $Qn\approx 1$ (L=3uH and C=100nF), while the second one employed a 10-times reduced filter capacitance value compared to the first one (C=10nF, $Qn\approx 0.9$). The RLC filter with the proposed method achieved the most beneficial results both at the load and the inverter sides, while the second one improved the filter efficiency by half. This indicates that the RLC filter also has a trade-off between voltage-overshoot level and filter efficiency due to the current variations, similar to what is observed in the RC filter.

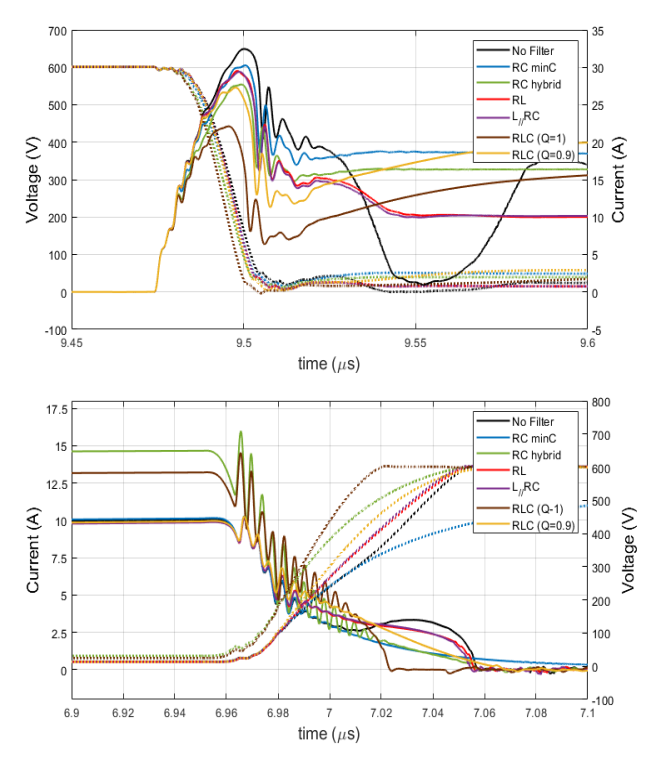


Fig. 9. Inverter Switch-On (top) and Switch-Off (bottom)

TABLE V SIMULATED FILTER PERFORMANCE RESULTS

	Load side		Iı	Filter		
Topology	V_L	dV/dt	E_{ON}	E_{OFF}	E_{loss}	E_R
	(p.u.)	(V/ns)	(uJ)	(uJ)	(%)	(mJ)
No Filter	1.914	54.35	232.69	80.89	-	-
RC minC	1.007	28.82	206.11	40.18	-21%	7.01
RC hybrid	1.034	28.16	176.92	83.144	-17%	7.45
RL	1.101	27.59	214.01	80.71	-6%	0.082
L//RC	1.066	26.63	213.73	80.85	-6.1%	0.078
RLC (Q=1)	1.013	5.53	146.67	85.21	-26%	7.87
RLC (Q=0.9)	1.048	5.12	201.48	75.45	-12%	3.26

CONCLUSION

The paper demonstrated the potential usage of a Smith chart to design passive RWP filters. By leveraging the properties of a Smith chart, the filter coefficients can be determined without the need for complex mathematical filter equations. Regarding impedance-matching, nearly perfect matching is achievable with RC filters if the load EPC values are met for the system. Similarly, RL filters would yield comparable matching results if sufficient inductance is applied to the filters against the load inductance. Additionally, the paper provided an example of finding the optimum RLC dV/dt filter coefficients for effective overvoltage damping.

There are still many ways to explore different topologies, such as T-network, Pi-network, as well as the combination of source-side filter and load-side filter. Based on the development of this graphical methodology, more complex filter topologies can be experimented with in the future.

APPENDIX A

The accuracy of the $\omega_{eq}=4/\pi T$ method is shown in Figs. 10 and 11, compared to Eq. (14c) and SPICE simulation. A 50-ohm, 50ns propagation delay cable was used in an open-circuit setup. RC filter had 0.1nF capacitor, RL filter had 1uH inductor. Each Γ was sweeping t up to 100ns (2td) to mimic period ($t_d \sim 3t_d$). Each 1st peak voltage $V_L(2td)$ aligned with Γ_N (MAPE less than 2%).

$$\begin{split} |\Gamma_{\omega_{eq}}| &= |\frac{-j/\omega_{eq}C_N}{2-j/\omega_{eq}C_N}| = \frac{1}{|2\omega_{eq}C_N - j|} = \frac{t}{\sqrt{t^2 + (\frac{8C_N}{\pi})^2}} \\ 1 + \Gamma_N &= (2 - e^{-\frac{t}{2C_N}}) \approx 1 + \frac{t}{\sqrt{t^2 + (\frac{8C_N}{\pi})^2}} = 1 + |\Gamma_{\omega_{eq}}| \end{split}$$

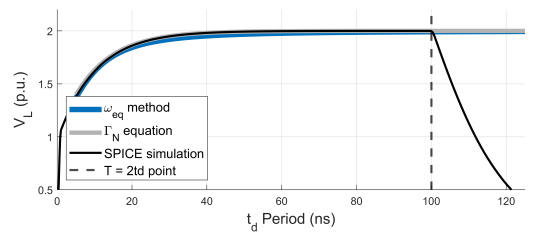


Fig. 10. An example $1 + \Gamma_L$ calculation with RC filter

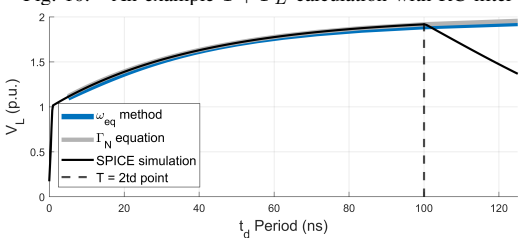


Fig. 11. An example $1 - \Gamma_S$ calculation with RL filter

APPENDIX B

In this study, the RLC filter was designed to achieve the minimum overvoltage at the cable output, rather than focusing on maximum filter efficiency. A comparison with literature methods for RLC coefficients is presented in Table VI. A 50-ohm, 20ns propagation delay cable condition was used.

TABLE VI RLC FILTER COEFFICIENTS COMPARISON

	Target V_L [p.u.]	R [Ohm]	L [uH]	C [nF]
RLC (Q=1)	1.01 (1%)	50	3	100
RLC (Q=0.9)	1.1 (10%)	50	3	10
RLC [3]	1.2 (20%)	50	4.1	22
RLC [16]	1.2 (20%)	50	8.2	13

REFERENCES

- Narayanasamy, Balaji, et al. "Reflected wave phenomenon in SiC motor drives: consequences, boundaries, and mitigation." IEEE transactions on power electronics 35.10 (2020): 10629-10642.
- [2] Finlayson, Paul T. "Output filters for PWM drives with induction motors." IEEE Industry Applications Magazine 4.1 (1998): 46-52.
- [3] von Jouanne, Annette, and Prasad N. Enjeti. "Design considerations for an inverter output filter to mitigate the effects of long motor leads in ASD applications." IEEE Transactions on Industry Applications 33.5 (1997): 1138-1145
- [4] Habetler, Thomas G., Rajendra Naik, and Thomas A. Nondahl. "Design and implementation of an inverter output LC filter used for dv/dt reduction." IEEE Transactions on Power Electronics 17.3 (2002): 327-331.

- [5] Zhang, Yu, Yanjun Shi, and Hui Li. "Study of passive dv/dt filter and proposed active solution for sic mv motor drive." 2019 IEEE Electric Ship Technologies Symposium (ESTS). IEEE, 2019.
- [6] Akagi, Hirofumi, and Itaru Matsumura. "Overvoltage mitigation of inverter-driven motors with long cables of different lengths." IEEE transactions on industry applications 47.4 (2011): 1741-1748.
- [7] Morya, Ajay Kumar, et al. "Wide bandgap devices in AC electric drives: Opportunities and challenges." IEEE Transactions on Transportation Electrification 5.1 (2019): 3-20.
- [8] K. Choksi, et al. "Evaluation of Factors Impacting Reflected Wave Phenomenon in WBG Based Motor Drives," 2022 International Power Electronics Conference (IPEC-Himeji 2022- ECCE Asia), Himeji, Japan, 2022, pp. 736-740.
- [9] Y. Wu, et al. "An Extendable and Accurate High- Frequency Modelling of Three-phase Cable for Prediction of Reflected Wave Phenomenon," 2022 IEEE Applied Power Electronics Conference and Exposition (APEC), Houston, TX, USA, 2022, pp. 944-950.
- [10] Smith, Phillip H. "Electronic applications of the Smith Chart: in waveguide, circuit, and component analysis." (No Title) (1969).
- [11] Gonzalez, Guillermo. "Microwave Transistor Amplifiers: Analysis and Design." United Kingdom, Prentice Hall, 1997.
- [12] Skibinski, G. "Design methodology of a cable terminator to reduce reflected voltage on AC motors." IAS'96. Conference Record of the 1996 IEEE Industry Applications Conference Thirty-First IAS Annual Meeting. Vol. 1. IEEE, 1996.
- [13] Moreira, Alessandro F., et al. "High frequency modeling for cable and induction motor overvoltage studies in long cable drives." Conference Record of the 2001 IEEE Industry Applications Conference. 36th IAS Annual Meeting (Cat. No. 01CH37248). Vol. 3. IEEE, 2001.
- [14] Weens, Yannick, Nadir Idir, and Jean-Jacques Franchaud. "Power cables models with frequency dependent parameters." Int Rev Electr Eng 2.6 (2007): 763-770.
- [15] Skibinski, Gary, David Leggate, and R. Kerkman. "Cable characteristics and their influence on motor over-voltages." Proceedings of APEC 97-Applied Power Electronics Conference. Vol. 1. IEEE, 1997.
- [16] Lee, SangCheol, and KwangHee Nam. "Overvoltage suppression filter design methods based on voltage reflection theory." IEEE Transactions on Power Electronics 19.2 (2004): 264-271.
- [17] von Jouanne, Annette, P. Enjeti, and W. Gray. "Application issues for PWM adjustable speed AC motor drives." IEEE Industry Applications Magazine 2.5 (1996): 10-18.
- [18] Tallam, Rangarajan M., et al. "Integrated differential-mode and common-mode filter to mitigate the effects of long motor leads on AC drives." IEEE Transactions on Industry Applications 47.5 (2011): 2075-2083.
- [19] Ruffo, Riccardo, et al. "Inverter side RL filter precise design for motor overvoltage mitigation in SiC-based drives." IEEE Transactions on Industrial Electronics 67.2 (2019): 863-873.
- [20] He, Jiangbiao, et al. "Multi-domain design optimization of dv/dt filter for SiC-based three-phase inverters in high-frequency motor-drive applications." IEEE Transactions on Industry Applications 55.5 (2019): 5214-5222.
- [21] Moreira, Alessandro F., et al. "High frequency modeling for cable and induction motor overvoltage studies in long cable drives." Conference Record of the 2001 IEEE Industry Applications Conference. 36th IAS Annual Meeting (Cat. No. 01CH37248), Vol. 3. IEEE, 2001.
- [22] Xu, Donglin, et al. "Design and Multi-constraint Evaluation of Passive dv/dt Filter for SiC-based Motor Drives." 2022 25th International Conference on Electrical Machines and Systems (ICEMS). IEEE, 2022.
- [23] Mirafzal, Behrooz, Gary L. Skibinski, and Rangarajan M. Tallam. "A failure mode for PWM inverter-fed AC motors due to the antiresonance phenomenon." IEEE Transactions on Industry Applications 45.5 (2009): 1697-1705.
- [24] Zhang, Zheyu, et al. "Decoupling of interaction between WBG converter and motor load for switching performance improvement." 2016 IEEE Applied Power Electronics Conference and Exposition (APEC). IEEE, 2016
- [25] Zobel, Otto J. "Theory and design of uniform and composite electric wave-filters." The Bell System Technical Journal 2.1 (1923): 1-46.
- [26] Li, Xiao, et al. "Impact of the Leakage Inductance on the Reflected Wave Phenomenon in MMC based Motor Drives." 2020 IEEE Applied Power Electronics Conference and Exposition (APEC). IEEE, 2020.
- [27] Mirza, Abdul Basit, et al. "An E-Core Based Integrated Coupled Inductor for Interleaved Boost Converter." IEEE Transactions on Industry Applications (2023).